ORIGINAL RESEARCH

Co-Delivery of Curcumin and Paclitaxel by "Core-Shell" Targeting Amphiphilic Copolymer to Reverse Resistance in the Treatment of Ovarian Cancer

Meng-Dan Zhao[1]
Jun-Qin Li[2]
Feng-Ying Chen[1]
Wei Dong[3]
Li-Juan Wen[4]
Wei-Dong Fei[1]
Xiao Zhang [ID][1]
Pei-Lei Yang[1]
Xin-Mei Zhang [ID][2]
Cai-Hong Zheng[1]

[1]Department of Pharmacy, Women's Hospital, Zhejiang University School of Medicine, Hangzhou 310006, People's Republic of China; [2]Department of Gynecology, Women's Hospital, Zhejiang University School of Medicine, Hangzhou 310006, People's Republic of China; [3]Department of Neurology, The Affiliated Yangming Hospital of Ningbo University, Yuyao People's Hospital of Zhejiang Province, Yuyao 315400, Zhejiang, People's Republic of China; [4]Institute of Pharmaceutics, College of Pharmaceutical Science, Zhejiang University, Hangzhou 310058, People's Republic of China

Correspondence: Xin-Mei Zhang;
Cai-Hong Zheng
Email zhangxinm@zju.edu.cn;
chzheng@zju.edu.cn

Background: Ovarian cancer is a common malignancy in the female reproductive system with a high mortality rate. The most important reason is multidrug resistance (MDR) of cancer chemotherapy. To reduce side effects, reverse resistance and improve efficacy for the treatment of ovarian cancer, a "core-shell" polymeric nanoparticle-mediated curcumin and paclitaxel co-delivery platform was designed.

Methods: Nuclear magnetic resonance confirmed the successful grafting of polyethylenimine (PEI) and stearic acid (SA) (PEI-SA), which is designed as a mother core for transport carrier. Then, PEI-SA was modified with hyaluronic acid (HA) and physicochemical properties were examined. To understand the regulatory mechanism of resistance and measure the anti-tumor efficacy of the treatments, cytotoxicity assay, cellular uptake, P-glycoprotein (P-gp) expression and migration experiment of ovarian cancer cells were performed. In addition, adverse reactions of nanoformulation to the reproductive system were examined.

Results: HA-modified drug-loaded PEI-SA had a narrow size of about 189 nm in diameters, and the particle size was suitable for endocytosis. The nanocarrier could target specifically to CD44 receptor on the ovarian cancer cell membrane. Co-delivery of curcumin and paclitaxel by the nanocarriers exerts synergistic anti-ovarian cancer effects on chemosensitive human ovarian cancer cells (SKOV3) and multi-drug resistant variant (SKOV3-TR30) in vitro, and it also shows a good anti-tumor effect in ovarian tumor-bearing nude mice. The mechanism of reversing drug resistance may be that the nanoparticles inhibit the efflux of P-gp, inhibit the migration of tumor cells, and curcumin synergistically reverses the resistance of PTX to increase antitumor activity. It is worth noting that the treatment did not cause significant toxicity to the uterus and ovaries with the observation of macroscopic and microscopic.

Conclusion: This special structure of targeting nanoparticles co-delivery with the curcumin and paclitaxel can increase the anti-tumor efficacy without increasing the adverse reactions as a promising strategy for therapy ovarian cancer.

Keywords: co-delivery, curcumin, reverse resistance, paclitaxel, ovarian cancer, adverse reactions

Introduction

Ovarian cancer is a common malignancy in the female reproductive system with a high mortality rate.[1] Because ovaries are located in the pelvic cavity, the symptoms are very subtle when a malignant tumor occurs. When patients feel uncomfortable, they have entered an advanced stage and foci become difficult to completely excise by operations. The standard treatment for advanced epithelial ovarian cancer consists of surgery and chemotherapy.[2] However, the primary purpose of surgery is to reduce the amount of

macroscopic tumor. Residual lesions require reliable chemotherapy to prompt the treatment. Although ovarian cancer is sensitive to the first-line chemotherapy regimens (such as paclitaxel), the effects are short-lived and drug resistance can be easily developed,[3] which makes a great clinical challenge to reduce ovarian cancer mortality. Due to genetic composition, a large number of tumors have the tendency to develop chemotherapy resistance during the preliminary therapy or even at the beginning. So, it is significant to find effective methods to reverse paclitaxel resistance in ovarian cancer.

Curcumin is a natural polyphenol compound that can be utilized as a nutraceutical or a pharmaceutical in functional foods, medicines and supplements.[4] It possesses multiple pharmacological properties, such as antioxidant, anti-inflammatory properties,[5] and has been shown to inhibit proliferation and survival of tumor cells.[6] In recent years, with the deepening of drug resistance research, it has been found that curcumin can improve the drug resistance of tumor cells by regulating a variety of signaling pathways and increase the sensitivity of drugs to a certain extent and reverse the resistance of tumors.[7] Meanwhile, curcumin could act as a chemopreventive agent involved in the progression of treatments which mitigates the off-target harmful impact of chemotherapy on the surrounding normal tissues and significantly inhibit cell pathway and induce apoptosis.[8] Cellular molecular targets involving re-sensitization of curcumin are also addressed when used with paclitaxel.[9] However, the application of curcumin is currently limited by its chemical instability, low water-solubility, and poor oral bioavailability. Nanoformulations of curcumin are rational methods to promote the stability in physiological media and improve bioavailability for improving the therapeutic benefit.[9,10] Kesharwani et al[11] described a polymer-based anti-inflammatory technology with curcumin specifically targeted to the luminal side of the colon, and the modified curcumin was >1000 times water soluble than curcumin. Kumar et al[12] studied that cationic copolymer can enhance the aqueous solubility, stability and bioavailability of curcumin and in vivo with mice the curcumin complexes increased peak plasma concentration of curcumin by 6 times and oral bioavailability by ~20 times.

Multifunctional nanoparticle offers many advantages in circumventing MDR due to their design, stability and selectivity in cancer microenvironment.[13] For example, nanocarrier can also improve the uptake of the drug into resistant tumor cell and reduce systemic toxicities, delivering a precise fraction of the drug to the tumor bed.[14] So, recently, polymeric micelle nanocarrier (self-assembled colloidal particles, with a hydrophilic head and a long hydrophobic tail, which enhance the solubility, permeability and bioavailability of drugs) has witnessed significant developments in cancer therapy.[15] At the same time, research points out that one of the effective approaches to improve the efficacy of chemotherapy and overcome MDR would be to employ a multifunctional approach (utilization of drug resistance modulators and combination therapy) using micelles as drug delivery systems.[15] We previously synthesized a biodegradable nanocarrier that specifically targets endometriosis.[16] Considering that ovarian cancer specifically expresses certain receptors, we will also modify the vector so that it can encapsulate paclitaxel and curcumin and target ovarian cancer.

Ovarian cancer tissues express a higher level of CD44, so pelvic peritoneum contains highly enriched CD44-positive cancer cells, driving tumor metastasis and responsible for tumor resistance to chemotherapy.[17] When CD44 was knocked down, proliferation, invasion activity, and spheroid formation were significantly suppressed and the drug sensitivity was enhanced. Thus, developing strategies to target CD44 may prevent metastasis and drug resistance in ovarian cancer. Hyaluronic acid (HA) is a polyanionic polysaccharide. It is biodegradable and biocompatible with low toxicity, and its products induce receptor-mediated intracellular signaling. Nanoparticles modified with HA would enable target into cancer cells based on its affinity with over-expressed CD44 on cancer cell membranes.[18]

In this study, we investigated biocompatible stearic acid (SA), an endogenous long-chain saturated fatty acid,[16] modified polyethylenimine (PEI) nanoparticles as a vehicle to co-delivery of paclitaxel and curcumin. The schematic (Scheme 1) provided a plausible mechanism for the putative anti-cancer effects. Such modifications can reduce the related disadvantages of PEI (cationic polyplex) as commonly used carriers. The amphiphilic graft copolymer (PEI-SA) consists of SA as a hydrophobic segment, PEI as a hydrophilic group and then HA was further coated as an "antibody-receptor" targeting group shell. The use of these nanoparticles strongly and synergistically enhances the cytotoxicity of paclitaxel. The mechanism of delivery of paclitaxel and curcumin by nanoparticle co-encapsulation showed that curcumin may inhibit the efflux of P-glycoprotein (P-gp) and may change the paclitaxel signaling pathway to enhance the synergistic effect of the drug combination. At the same time, there is no obvious effect on normal tissues. We believe that targeted (PEI-SA)HA of co-encapsulation platforms for paclitaxel
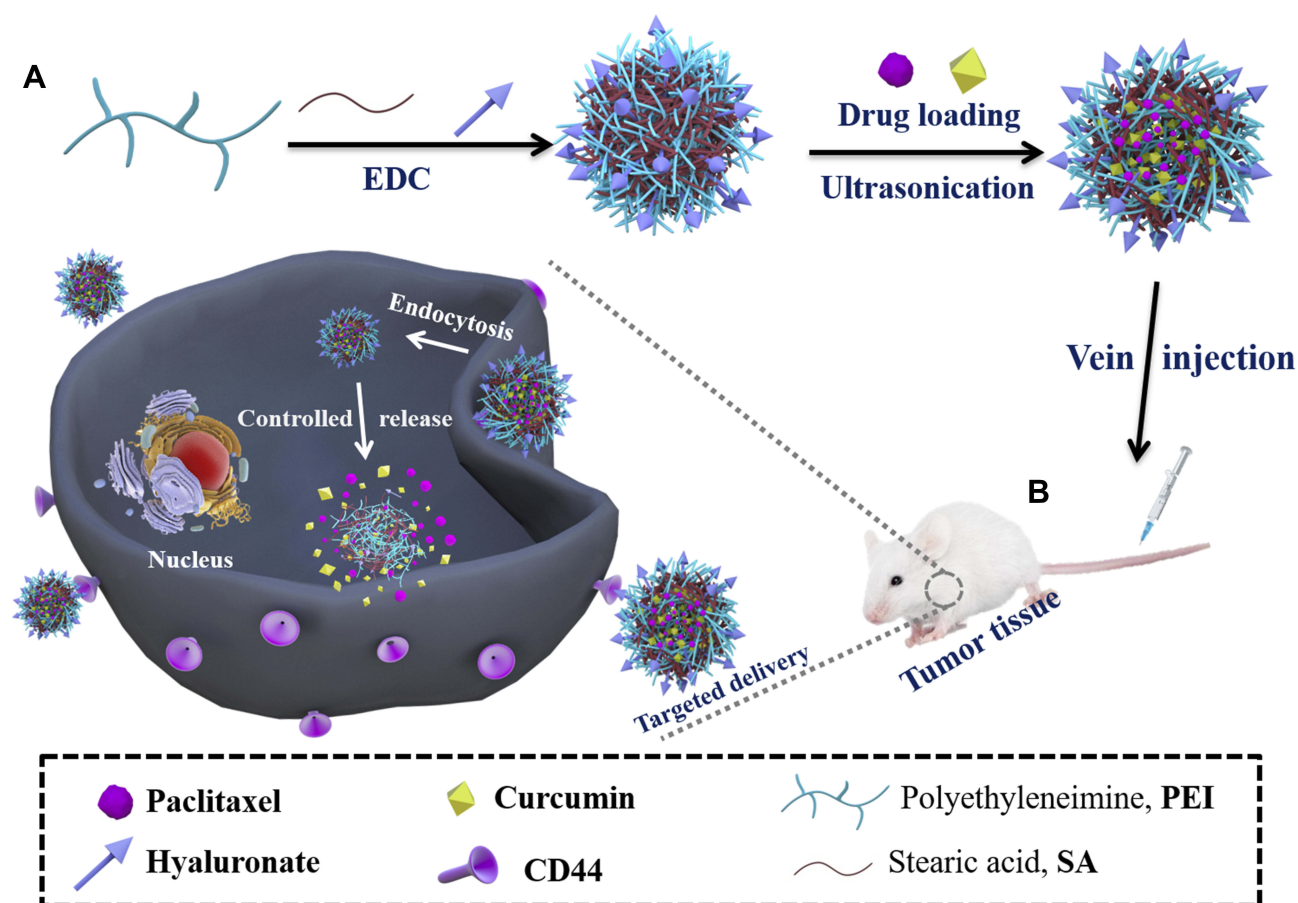
Scheme I Schematic representation of the nanoparticles in ovarian cancer tissue microenvironment. (**A**) Preparation of drug-loaded nanoparticles; (**B**) In vivo treatment process.

and curcumin has broad potential to be used in ovarian cancer therapy.

Materials and Methods
Materials
Stearic acid was provided by Shanghai Chemical Reagent Co. Ltd (Shanghai, China); polyethylenimine (branched, 10 kDa), sodium hyaluronate (10 kDa) and 3-(4, 5-dimethyl-thiazol-2-yl)-2,5-diphenyl-tetrazolium bromide (MTT) were purchased from Sigma (St Louis, MO, USA); 1-ethyl- 3-(3-dimethylaminopropyl) carbodiimide (EDC) and 2,4,6-trinitrobenzene sulfonic acid (TNBS) were purchased from Sigma (St Louis, MO, USA); paclitaxel (PTX) was gifted from Zhanwang Biochemical Co., Ltd. (Huzhou, China); curcumin was provided by Aladdin Reagent Co., Ltd. (Shanghai, China); Dulbecco's modified Eagle's medium (DMEM) and trypsin-EDTA were purchased from Gibco (BRL, MD, USA); fetal bovine serum (FBS) was purchased from Sijiqing Biologic Co., Ltd. (Zhejiang, China); fluorescein isothiocyanate (FITC)

and rhodamine isothiocyanate (RITC) were purchased from Guangzhou Zhanchen Biotech Co., Ltd. (Guangzhou, China); all other solvents and reagents were of analytical grade and used without further purification.

Preparation and Characterization of (PEI-SA)HA Micelles
The carboxyl group of SA and the primary amine group of PEI are dehydrated and condensed to obtain PEI-SA, with an activator of a carboxyl group EDC. A quantity of 199 mg SA was pre-dissolved in 50 mL hot ethanol, and 500mg PEI was dissolved in 40 mL distilled water, respectively. Then, they were mixed at 80 °C under stirring. Then, 750 mg EDC was added into the mixture under stirring with 300 rpm, lasting for 24 hrs. The reaction solution was dialyzed against a 10% ethanol solution for 48 hrs using a dialysis membrane (MWCO: 3.5 KDa, Spectrum Laboratories, Laguna Hills, CA) to remove by-products. Finally, it was dialyzed against distilled water for 2 hrs, and the dialyzed product was lyophilized, and PEI-SA was collected. Then

the solutions of PEI-SA were coated by HA with different concentrations to obtain (PEI-SA)HA micelles.

The degree of substitution (SD) of (PEI-SA)HA was determined by the TNBS method, which refers to the number of stearic acid groups per PEI of 100 amino groups.[16] Briefly, 2 mL of 4% $NaHCO_3$ and 2 mL of 0.1% TNBS solution were added to 2 mL of a (PEI-SA) HA solution containing 125 µM of (PEI-SA)HA, and the mixture was incubated at 37 °C for 2 hrs. Then, 2 mL of 2N HCl solution was added to the mixture to neutralize the $NaHCO_3$ residue. The final reaction mixture was measured by UV spectroscopy (TU-1800 PC, Beijing Purkinje General Instrument Co., Ltd., China) to set the absorbance at 344 nm. The SD of the (PEI-SA)HA is calculated from a calibration curve obtained from the PEI solution.

The critical micelle concentration (CMC) of (PEI-SA) HA was determined by fluorescence measurement with hydrazine as a probe. The excitation wavelength was 336 nm and the erbium emission was monitored over a wavelength range of 360–455 nm and was recorded on a fluorometer (F-2500, HITACHI Co., Japan) at room temperature. The concentration of the PEI-SA solution containing 5.93×10^{-7} M oxime varied from 1.0×10^{-4} to 1.0 mg/mL. Based on the erbium emission spectrum, the intensity ratio of the first peak (I_1, 375 nm) to the third peak (I_3, 384 nm) was analyzed to calculate CMC.

Preparation and Characterization of Drug Loaded (PEI-SA)HA Micelles

PTX and curcumin loaded in (PEI-SA)HA micelles were prepared using probe-type ultrasonication according to our previous report.[19] (PEI-SA)HA (10 mg) was dissolved in 2 mL distilled water, and then 0.8mL PTX and curcumin (1 mg/mL) ethanol solution were added to micelle solution slowly under stirring at room temperature and then the mixture was ultrasonicated for 15 mins (JY92-II, Ningbo Xinzhi Scientific Instrument Institute, Zhejiang, China) in the ice bath. After that, the mixture was stirred for 4 hrs, followed by dialysis against pure water overnight using a dialysis membrane (MWCO: 7000 Da, USA). Fresh distilled water was exchanged frequently. Then, the solution was centrifuged at 3500 rpm for 15 mins (3K30, Sigma Laborzentrifugen, USA) to remove unloaded PTX and curcumin and then filtered with a 0.45 µm pore-sized filter and lyophilized (Labconco, Freezone 2.5 Plus, USA), and the product of (PEI-SA)HA micelles with PTX and curcumin loaded (abbreviation for (PEI-SA)HA/PC) was obtained.

The average hydrodynamic diameter of (PEI-SA)HA complex and drug-loaded (PEI-SA)HA micelles was measured by dynamic light scattering with a Zetasizer (3000HS, Malvern Instruments Ltd., UK). The morphological examination of (PEI-SA)HA complex and drug-loaded (PEI-SA) HA micelles was observed by transmission electron microscopy (TEM, JEOL, JEM2100, Japan).

Cell Culture

Human ovarian cancer cells (SKOV3) and multi-drug resistant variant (SKOV3-TR30) were obtained from Women's Hospital, College of Medicine, Zhejiang University (Hangzhou, China), and the use of the cell lines was approved by the institutional ethics committee of Women's Hospital, College of Medicine, Zhejiang University. Cells were cultivated in DMEM supplemented with 10% (v/v) fetal bovine serum and penicillin/streptomycin (100 units/ mL, 100 units/mL) at 37°C with 5% CO_2.

P-gp Expression on Cells

To check whether P-gp was expressed on the cell surface, incubate 1×10^6 cell suspension in 200 µL phosphate buffer solution (PBS containing 0.1% NaN3 and 1% bovine serum albumin, pH 7.4) at 4 °C for 30 mins and with monoclonal MRK-16 mouse antibody against P-gp. After washing the cells with ice-cold PBS, the cells were centrifuged to remove unbounded antibody and re-suspended in fresh PBS. Cells were again incubated with goat anti-mouse IgG fluorescein conjugate for 30 mins at a working dilution of 1:50 at 4 °C.

In vitro Cytotoxicity Assay

The experiment observed that living cells converted the soluble tetrazolium salt 3-(4,5-dimethyl-2-tetrazolyl)-2,5-diphenyl-2H tetrazolium bromide (MTT) into insoluble alpha crystals. Briefly, 1×10^4 SKOV3 and SKOV3-TR30 cells taken from the culture index period were grown in 180 µL medium in 96-well plates and cultured for 1 day at 37°C and 5% CO_2. In addition, cells were exposed to different concentrations of PTX, curcumin, (PEI-SA)HA/PTX, (PEI-SA)HA/curcumin and (PEI-SA)HA/PC at 37°C, lasting for 48 hrs. At the end of the incubation time, 20 µL of MTT solution was added and incubated additionally at 37 °C for 4 hrs. The medium was then replaced with 150 µl of DMSO to dissolve the MTT formazan crystals. Finally, the plate was shaken for 20 mins and the absorbance of the product was

measured at 570 nm in a microplate reader (BioRad, Model 680, USA). The percentage of cell survival was calculated as compared to mock-treated cells (100% survival). All experiments were performed in triplicate. The same method was also used to assess the cytotoxicity of (PEI-SA)HA.

Observation of Internalization of the Drug-Loaded Micelles

(PEI-SA)HA/PC micelles were labeled with FITC or RITC to investigate the intracellular distribution of drug-loaded micelles. Briefly, FITC- or RH-labeled (PEI-SA)HA/PC was prepared by dropwise addition of a FITC ethanol solution or RH to a (PEI-SA)HA/PC solution having a concentration of 1.0 mg/mL (PEI-SA)HA/PC. The molar ratio of (PEI-SA) HA/PC to FITC or RH was controlled at 1:4. After stirring at 400 rpm for 24hrs in a sterile environment at room temperature, the reaction product was dialyzed against distilled water for 24 hrs using a dialysis membrane (MWCO: 3.5 KDa, Spectrum Laboratories, Laguna Hills, CA) to remove unreacted FITC or RH and then the dialyzed product was lyophilized. SKOV3 cells were seeded for 24 hrs, placed in 24-well plates in 1 mL DMEM, and then incubated with FITC-labeled (PEI-SA)HA/PC or RITC-labeled (PEI-SA) HA/PC for 0–8 hrs. After washing three times with PBS, the cells were observed by a confocal microscope (Olympus America, Melville, NY).

Migration Experiment

Transwell method is used to study the influence of (PEI-SA) HA/PC and PTX on the SKOV3 and SKOV3-TR30 cell migration. Briefly, the cells were treated with (PEI-SA) HA/PC or PTX for 36 hrs, then they were re-suspended in 200 µL (25×10^5 cells/mL) serum-free culture medium containing (PEI-SA) HA/PC or PTX, and planted in the upper chamber. A quantity of 500 µl culture medium containing 10% FBS was added to the bottom well, then incubated at 37°C for 12 hrs. The cells non-migrated on the upper surface of the filter were gently removed with a cotton swab, and the cells that migrated into the underside of the filter were fixed and stained with crystal violet. Each experiment was performed in triplicate, and five randomly selected fields were counted per insert.

In vivo Distribution of Real-Time Imaging and Anti-Tumor Activity

In vivo distribution was determined by real-time fluorescence imaging. Nude mice were supplied by the Laboratory Animal Center of Zhejiang University. All experiments were performed in accordance with the guidelines for the care and use of animals established by Zhejiang University and in vivo experiments were approved by the animal ethics committee of Zhejiang University. All surgeries were performed under sodium pentobarbital anesthesia, and all efforts were made to minimize suffering. All animals were followed by the guidelines of the National Institutes of Health guide for the care and use of laboratory animals (NIH Publications No. 8023, revised 1978). A subcutaneous xenografted ovarian cancer model was established by subcutaneous inoculation of 5.0×10^6 SKOV3 cells in 100 µL of serum-free medium on the right side of female BABL/c nude mice (6-8w), and placed in a standard micro-isolator. Near-infrared dye ICG was physically encapsulated to trace the nanoparticle in vivo according to the method as described in the published literature.[20] The tumor growth-suppressing activity was evaluated by the tumor size at predetermined times with digital caliper after administration, and the tumor size and body weight of every mouse were measured every two days after the first injection. Tumor volume (mm^3) was calculated using the formula: volume = (width^2×length)×0.5. When the tumor reached a uniform size, the ICG-loaded (PEI-SA)HA/ICG polymeric nanoparticles were injected via the tail vein of tumor-bearing mice to detect the tumor distribution efficacy in the live animals. At predetermined time points (12 hrs, 24 hrs, 36 hrs, 48 hrs, 72 hrs), the mice were observed under a Maestro in vivo Imaging System (CRI, Woburn, MA). The fluorescence images of the excised organs and tumor tissues were also obtained by IVIS Spectrum.

A nude mouse model carrying the tumor was established with SKOV3 cell line as described above. When the tumor size is about 200 mm^3, the tumor-bearing mice were randomly divided into 7 groups and each group consisted of three mice. Different treatment groups were treated with 200 µL of free PTX, (PEI-SA)HA/PTX, free curcumin, free PTX combined free curcumin, (PEI-SA)HA/curcumin and (PEI-SA)HA/PC via tail vein, respectively. Each tumor-bearing mouse received the same dose (each dose contains 10 mg/kg PTX or curcumin) every other day for five times. Saline group, as a negative control, was given 200 µL of sterile normal saline with IV injection. The tumor growth inhibitory activity was evaluated by tumor size at a predetermined time after administration with a digital caliper, and the tumor size and body weight of each nude mouse were measured every two days after the first injection. Tumor volume (mm^3) was calculated using the following formula: volume = (width^2×length)×0.5.

Observation of Reproductive Organs by Transmission Electron Microscopy

Transmission electron microscopy was performed to examine whether (PEI-SA) HA/PC caused changes in apoptosis of uterine and ovarian structural cells. The uterus and ovaries were removed and fixed in 2.5% glutaraldehyde overnight in a refrigerator and washed in phosphate-buffered saline (pH 7.2) for 15 mins and 3 times. It was then placed in 1% osmium tetroxide for 1 h and washed 3 times. Thereafter, the sample was stained in 4% uranyl acetate for 30 mins, then dehydrated by a serial concentration of ethanol and embedded in a resin mixture (70, 80, 90, 95% ethanol, each for 10 mins). They were sectioned and observed under a TECNAI-10 transmission electron microscope (Phillips). Simultaneously verified by hematoxylin–eosin (HE) staining as previous literature.[21]

Statistical Analysis

Data were expressed as means of the three separate experiments and compared by the analysis of Graphpad prism 7.0. A p-value < 0.05 was considered statistically significant in all cases.

Results

Characteristics of PEI-SA Micelles

The PEI-SA prepared by the EDC method is shown in Figure 1A and ^{1}H NMR spectra of SA, PEI and PEI-SA are shown in Figure 1B, where the characteristic absorption peak of SA is 1.25–1.35 ppm position, marked with "a". The characteristic peak of SA is mainly produced by a long-chain methylene group. The characteristic absorption of PEI is marked with "b", located at 2.6–2.8 ppm, and the characteristic peak is mainly generated by the (-NHCH$_2$CH$_2$-) repeat structure of PEI. Comparing the NMR spectra of SA and PEI, two characteristic peaks of "a" and "b" can be found in the spectrum of PEI-SA, indicating that the synthetic product PEI-SA contains both the long-chain methylene structure in SA and the (-NHCH$_2$CH$_2$-) repeat structure in PEI. This further illustrates that PEI has been coupled to SA. The SD of PEI-SA was about 15.5% as shown in Figure 1C. The size distribution of PEI-SA was 135 nm on average as shown in Figure 1D. The CMC value of PEI-SA was about 0.024 mg/mL.

Characteristics of (PEI-SA)HA/PC

The volume average diameter sizes of the various particles are shown in Table 1. The average size of (PEI-SA)HA with 1 mg/mL was 165.28 nm with 0.267 polydispersity index. After the PTX and curcumin loading, the diameter was 189.65 nm with 0.252 polydispersity index for (PEI-SA)HA/PC. When the FITC labeled the (PEI-SA)HA/PC, the volume average diameter size was 187.77 nm with 0.268 polydispersity index, and 201.48 nm with 0.278 index when RH labeled the (PEI-SA)HA/PC. There was no obvious difference in diameter after the drug loading. The transmission electron microscopy images are shown in Figure 2 (A was (PEI-SA)HA and B was (PEI-SA)HA/PC). The particle sizes from the transmission electron microscope images were consistent with that obtained using dynamic light scattering measurements.

P-gp Expression and Cytotoxicity Assay

P-gp expression on SKOV3/SKOV3-TR30 cells was confirmed by qualitative flow cytometry. Binding of MRK-16 to P-gp was detected in the SKOV3-TR30 cells. The SKOV3-TR30 showed fluorescence peaks at about 228.2 and 151.0, respectively, and the sensitive cells were at 5.7 and 6.3, respectively. The difference of fluorescence signals between sensitive and resistant cells treated with only secondary antibody was negligible which indicated minimal nonspecific interactions of the secondary antibody with the cells. After treatment with (PEI-SA)HA/PC, it can effectively downregulate the expression of related P-glycoprotein (P-gp) in SKOV3-TR30 cells.

The IC$_{50}$ of (PEI-SA)HA against SKOV3 was 478 μM which indicated that the (PEI-SA)HA had relatively low cytotoxicity.

In SKOV3 Cells, the IC$_{50}$ of free PTX was 1.35 μM, while the IC$_{50}$ loading in (PEI-SA)HA was 0.11 μM (as shown in Table 2). The free curcumin had an IC$_{50}$ of 2.49 μM and an IC$_{50}$ was 0.68 μM when mediated by the (PEI-SA)HA vector. The effect of simple PTX combined (PEI-SA) HA/curcumin on drug-resistant cells is similar to that of sensitive cells. When both PTX and curcumin were loaded in the (PEI-SA)HA carrier ((PEI-SA)HA/PC), the IC$_{50}$ was smaller, indicating that the two drugs have a synergistic effect. In SKOV3-TR30 Cells, the IC$_{50}$ of free PTX was 9.33 μM, while the IC$_{50}$ loading in (PEI-SA) HA was 0.13 μM. The free curcumin had an IC$_{50}$ of 3.83 μM and an IC$_{50}$ was 0.70 μM when mediated by the (PEI-SA)HA vector. (PEI-SA)HA/PC showed the best cytotoxicity on SKOV3-TR30 cell lines.

The toxicity of free PTX to drug-resistant cells was significantly reduced. PTX was effectively mediated by
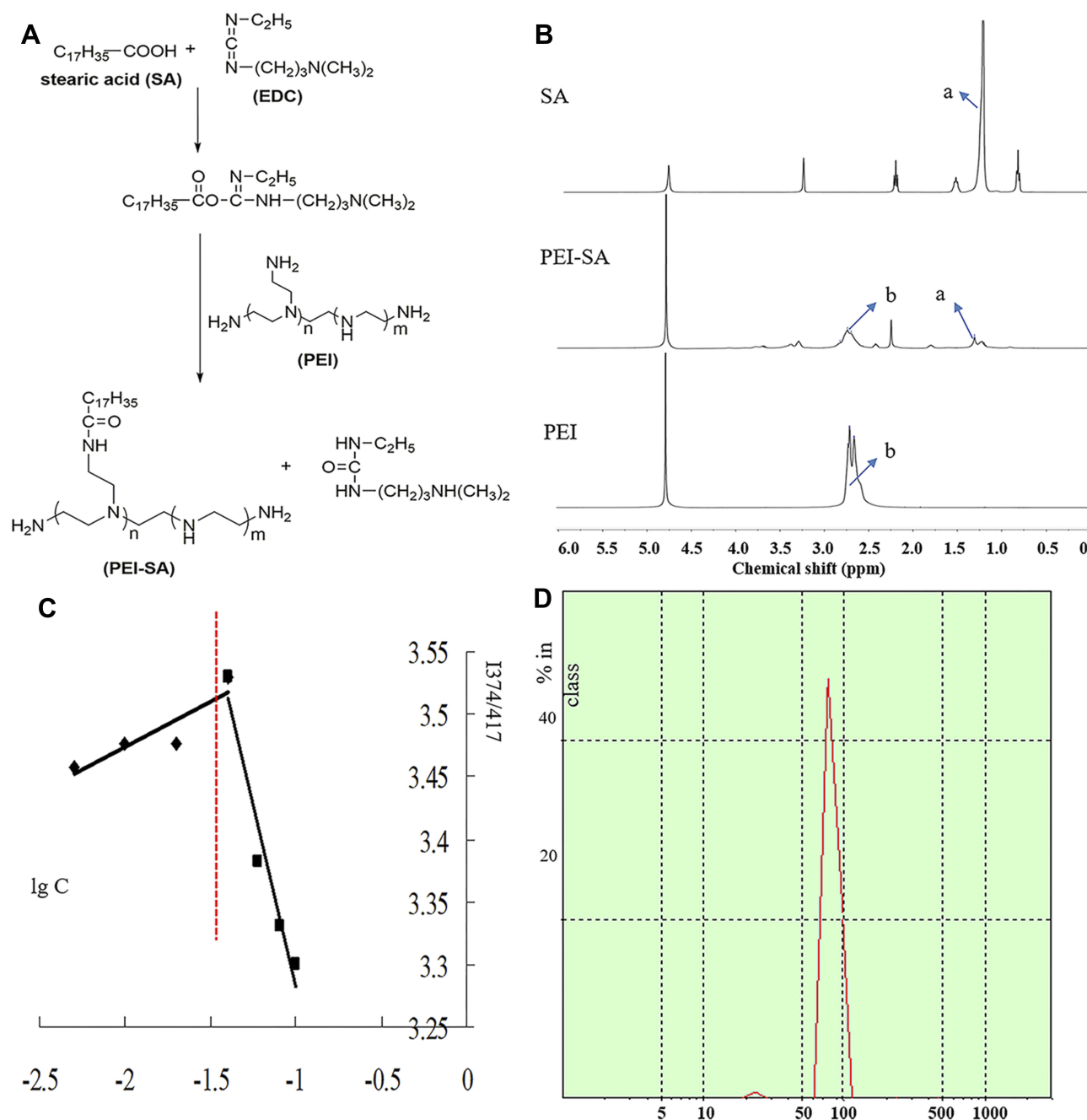
Figure 1 Synthesis and characterization of PEI-SA complexes. (**A**) Scheme of EDC-mediated coupling reaction between PEI and SA. (**B**) ^{1}H NMR spectra of SA, PEI and PEI-SA. (**C**) Change of fluorescence intensity ratio (I_{374}/I_{417}) for pyrene in distilled water in the presence of PEI-SA with 15.5% substitute degrees of amino group. (**D**) The size distribution of PEI-SA.

(PEI-SA)HA against both sensitive and resistant cells. Curcumin has a similar effect on sensitive cells and drug-resistant cells after vector-mediated. This shows, on the one hand, the power of (PEI-SA) HA can effectively improve the effect of PTX on drug-resistant cells. On the other hand, the combination of curcumin and PTX has a stronger toxic effect on drug-resistant cell lines. Third,

the involvement of (PEI-SA)HA/curcumin reverses the role of PTX in drug-resistant SKOV3-TR30 cell lines.

Cellular Uptake
Cellular uptake was estimated in SKOV3 cells by fluorescence measurement using fluorescently labeled (PEI-SA)HA/PC. Figure 3 shows fluorescence microscopy images of

Table 1 The Volume Average Diameter Sizes of the Various Particles

Materials	Particle Size (nm)	PDI
(PEI-SA)HA	165.28±25.17	0.267±0.067
(PEI-SA)HA/PC	189.65±66.28	0.252±0.044
FITC-(PEI-SA)HA/PC	187.77±33.35	0.268±0.033
RH-(PEI-SA)HA/PC	201.48±36.88	0.278±0.031

Note: Data are represented as mean ± SD (n=3).
Abbreviation: PDI, polydispersity index.

FITC-labeled complexes and RITC-labeled complexes incubated with SKOV3 cells for 0, 1, 2, 4 and 8 hrs. As the incubation time increases, the fluorescence intensity gradually increases. Significant fluorescence was detected in all cells after 24 hrs. It is worth noting that the intracellular condition of fluorescence intensity in SKOV3-TR30 cells is similar to SKOV3. In addition, intracellular uptake of the fluorescently labeled complex is also performed in a quantitative manner. The mean fluorescence intensity of (PEI-SA)HA/PC was measured by flow cytometry after 4 hrs of incubation. The mean fluorescence index in SKOV3 cells was 18.4±2.1, and the mean fluorescence index in SKOV3-TR30 cells was 19.3 ±2.9. There is no significant difference (P>0.5). Mean fluorescence index was calculated as (fluorescence (test)-fluorescence (isotype control))/(fluorescence isotype control).

Migration Experiment

Transwell assays were studied to evaluate the therapeutic potential of the (PEI-SA)HA/PC (Figure 4). From the experimental results, the cell invasiveness of the sensitive cells (SKOV3) and the drug-resistant cells (SKOV3-TR30) are different. However, PTX significantly reduced the cell invasiveness of SKOV3, but it could hardly change the invasiveness of the drug-resistant cell SKOV3-TR30. (PEI-

SA)HA/PC inhibited the cell invasiveness of SKOV3 and SKOV3-TR30 significantly. The cell apoptosis and metastasis were inhibited in a dose-dependent manner, which was consistent with the reported views.[22,23] Therefore, (PEI-SA) HA/PC is effective not only for the treatment of SKOV3 cells but also for the resistant cell line SKOV3-TR30. This result is also consistent with the above cytotoxicity test, P-glycoprotein experimental results.

In vivo Distribution Studies in Tumor-Bearing Mice

Figure 5 is a graph showing the real-time distribution of the nanoparticle material in the animal. As can be seen from Figure 5A, most of the fluorescence was concentrated in the tumor site (the right side of female BABL/c nude mice) after the (PEI-SA) HA/ICG tail vein injection (12–72 hrs), and the free ICG entered the body 12 hrs later, mainly concentrated in the liver, and the fluorescence of the liver disappeared after 24 hrs, indicating that the free ICG was mainly eliminated in the liver after entering the body, and could not be applied to other parts such as tumors. This indicated that (PEI-SA) HA can be better targeted to the tumor site after entering the body. In order to further confirm the targeting of the vector, we also studied the fluorescence intensity of each tissue organ with qualitative (Figure 5B) and quantitative determination (Figure 5C) at the last 72 hrs. From the results, the fluorescence intensity of (PEI-SA) HA/ICG in tumors is much greater than that of free ICG. Although the fluorescence of (PEI-SA)HA/ICG is the strongest at the tumor site, the fluorescence intensity of (PEI-SA)HA/ICG in the liver is similar to that of the tumor site (P>0.05). This may be that the total volume of the liver is larger than that of the tumor, and the quantitative results of fluorescence are
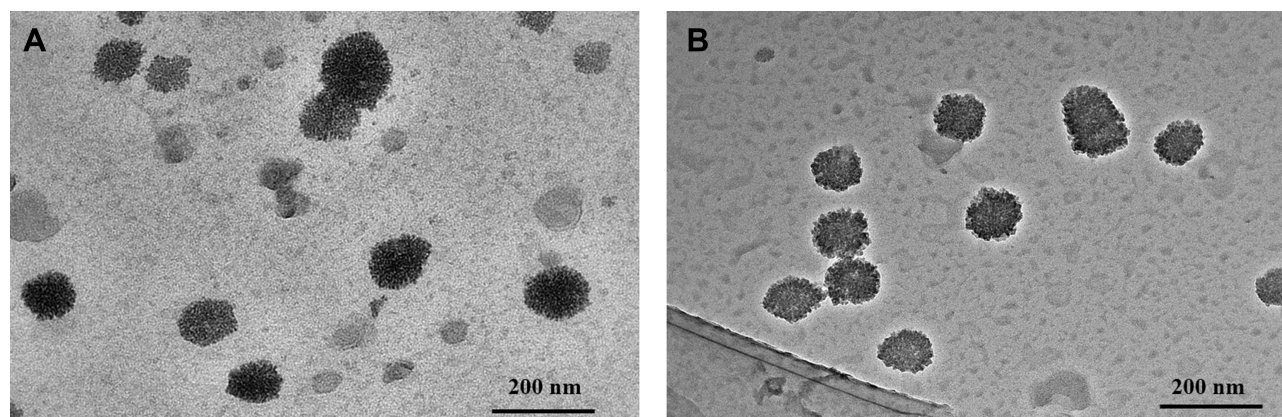

Figure 2 The transmission electron microscope images of (PEI-SA)HA (**A**) and (PEI-SA)HA/PC (**B**).

Table 2 The IC$_{50}$ Values of PTX, (PEI-SA)HA/PTX, Curcumin, (PEI-SA)HA/Curcumin and (PEI-SA)HA/PC Against SKOV3/SKOV3-TR30 Cells

Cell Line Material	IC$_{50}$ N= 3 (μM ± SD)	
	SKOV3	SKOV3-TR30
PTX	1.35±0.04	9.33±0.05
(PEI-SA)HA/PTX	0.11±0.003	0.13±0.003
Curcumin	2.49±0.50	3.83±0.49
PTX+(PEI-SA)HA/curcumin	0.45±0.050	0.53±0.070
(PEI-SA)HA/curcumin	0.68±0.018	0.70±0.020
(PEI-SA)HA/PC	0.078±0.002 (Calculated by PTX)	0.081±0.003 (Calculated by PTX)

deviated from the qualitative observation. Overall, (PEI-SA) HA/ICG has significant tumor targeting.

Treatment Effect

The results of animal treatment are shown in Figure 6. To further illustrate the efficacy experiments in vivo, we also compared free PTX, (PEI-SA)HA/PTX, free curcumin, free PTX combined free curcumin and (PEI-SA)HA/curcumin. As can be seen from Figure 6A, the groups of free curcumin and (PEI-SA) HA/curcumin are basically similar to the saline group, and the PTX, (PEI-SA) HA/PTX and PTX combined curcumin groups also have a certain therapeutic effect, but inferior to (PEI-SA) HA/PC. This indicates that (PEI-SA)HA/PC has a superior therapeutic effect on ovarian cancer tumors. After treatment, the overall weight of the nude mice did not differ significantly between the seven groups (since there was no significant

difference in body weight changes between the 7 groups, in order to observe the data more concisely and visually, only the saline and (PEI-SA) HA/PC groups are listed in Figure 6B). Moreover, the tumor tissue visually observed from the (PEI-SA)HA/PC group was significantly smaller than that of the saline group, and the weight of the tumors in the two groups was significantly different.

Discussion

At present, many derivatives of PEI have been synthesized. Many studies have shown that the modification of cationic polymers with hydrophobic groups can significantly change their physicochemical and biological properties, including increasing the encapsulation of drug, enhancing the adsorption of cells, reducing the effect of serum on transfection efficiency, reducing cell toxicity[24,25] and reversing drug resistance, and so on.[26,27]

How is the targeting of (PEI-SA)HA produced in this study? First, due to the composition and special spatial structure of (PEI-SA)HA. The hydrophilicity of PEI and the hydrophobicity of SA make (PEI-SA)HA have an amphiphilic structure, and the modification of the alkyl chain allows it to adhere to the biofilm.[28] Second, it is also possible to form a "secondary core" core-shell structure due to the structure of the PEI backbone and the shorter graft chain of SA, which is advantageous for the escape lysosome phagocytosis.[29,30] The nanoparticle size we prepared is suitable for the enhanced permeability and retention effect (EPR), allowing it to enter only the neovascularization.[31,32] Third, there is a relatively high expression of CD44 in the ovarian cancer tumor site. As
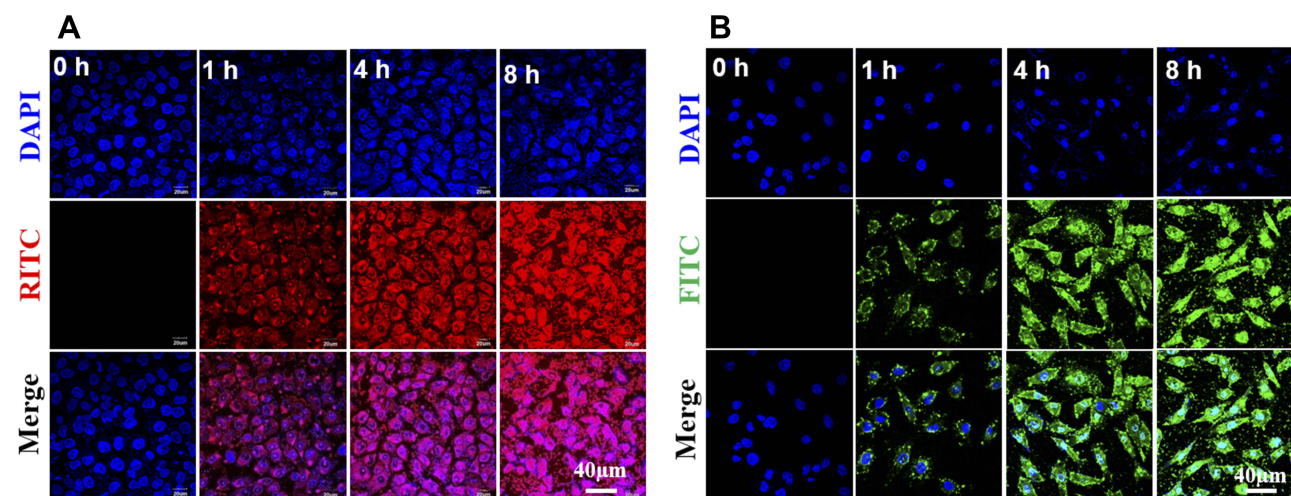

Figure 3 Fluorescence image observations. (**A**) Fluorescence image observations of the RITC-labeled (PEI-SA)HA/PC incubated with the SKOV3 cells for 0, 1, 4 and 8 hrs. (**B**) Fluorescence image observations of the FITC-labeled (PEI-SA)HA/PC incubated with the SKOV3 cells for 0, 1, 4 and 8 hrs. ×200 magnification.
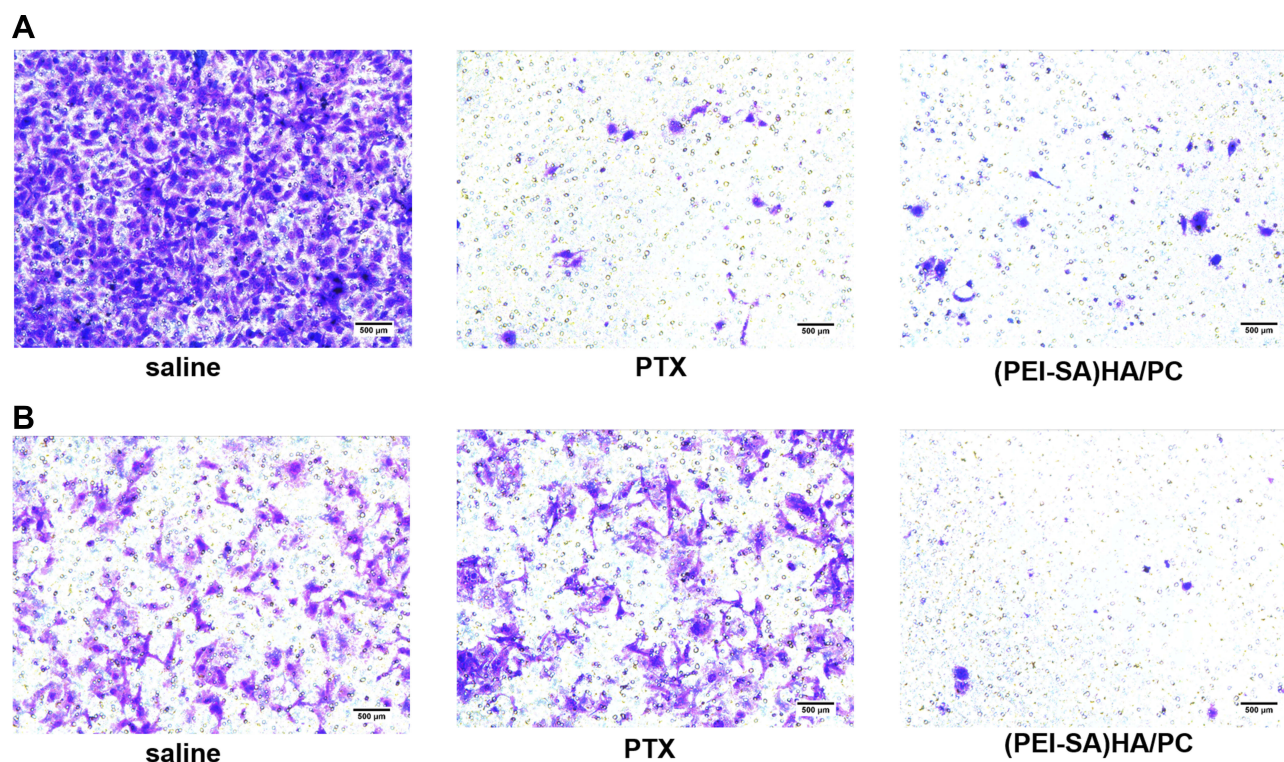
Figure 4 The invasiveness of SKOV3 and SKOV3-TR30 cells. (**A**) Representative photomicrographs of invasion with saline, PTX and (PEI-SA)HA/PC in SKOV3. (**B**) Representative photomicrographs of invasion with saline, PTX and (PEI-SA)HA/PC in SKOV3-TR30. Results are combined data from five experiments with different cell preparations. In SKOV3, both PTX and (PEI-SA) HA/PC significantly inhibited cell migration (P <0.001), which was significantly different from saline. In SKOV3-TR30, (PEI-SA) HA/PC significantly inhibited cell migration, but there was no significant difference between PTX and normal saline (P>0.05).

HA can specifically bind to CD44,[33–35] in vivo (PEI-SA) HA can specifically target the distribution of tumor tissue.

And why is there such a good anti-ovarian cancer effect? First of all, PTX is a microtubule-stabilizing and it is one of the most potent anti-ovarian cancer agents, but its clinical application is limited by multidrug resistance (MDR) and side effects.[36] (PEI-SA)HA provides unique physicochemical properties thereby improving the pharmacokinetics, pharmacodynamics, and biodistribution of the drug.[13] It reduces the amount of free drug in the circulation thereby limiting the passage of drug to the nontarget tissues and cells which overcome the drug resistance in tumors. Second, nanoparticles could reverse PTX resistance significantly by suppressing the over-expression of P-gp. As with our experimental results, P-gp in SKOV3-TR30 cells was significantly elevated and it can inhibit the expression of P-gp efflux mediated by (PEI-SA) HA/PC. This resulted in an increase in intracellular drug accumulation and a decrease in drug efflux in SKOV3-TR30 cells, which showed a good anticancer effect.

The results of its migration experiment also verify this (Figure 4). In addition, it may be that PTX and curcumin produce synergistic anti-cancer effects.[37] From the experimental results, PTX and curcumin exert potent anti-ovarian cancer effects in vitro and can help reduce dosage and minimize side effects of cytotoxic therapies. The combined treatment with PTX and curcumin resulted in a higher level of apoptosis compared with either substance alone. The study results of the synergy between the PTX and curcumin are similar to those reported in the literature.[38–40] This may be due to the inhibition of apoptosis and necrosis by PTX and curcumin, which is confirmed by various methods including caspase-3/7 activity, annexin V, caspase-3 protein and so on.[41] Therefore, rational design of synergistic drug-based regimens is essential to increase therapeutic efficacy and reduce toxic effects. At the same time, the co-delivery can reduce the amount of the carrier in addition to the synergistic effect compared to the respective encapsulated PTX and curcumin,[42] and the preparation is relatively convenient.

Any drug has duality, which is both beneficial and unfavorable to the body. To investigate whether (PEI-SA) HA/PC has an effect on normal reproductive organs (uterus and ovaries), we used electron microscopy and hematoxylin–eosin (HE) staining to analyze differences between tissues. There was no significant difference in
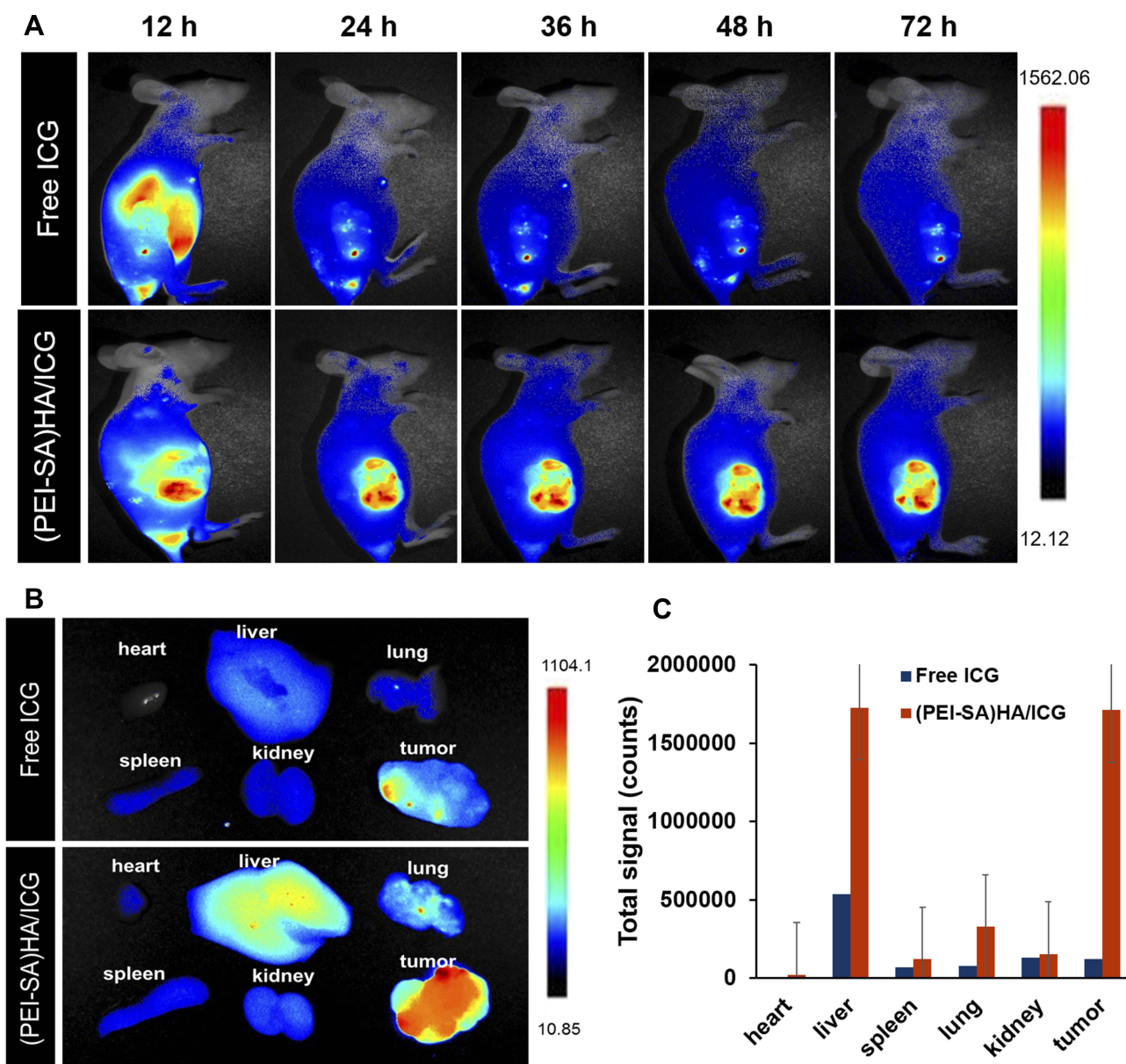
Figure 5 (**A**) Real-time fluorescence distribution of NPs in animals with respect to administration at different time points (12, 24, 36, 48, 72 h). (**B**) The fluorescence distribution of various tissues and organs of animals after 72 h. (**C**) The quantitative determination of the fluorescence intensity of tissues and organs after 72 h.

weight of the ovaries and intact uterus between the (PEI-SA)HA/PC group and the saline group. The genital index analysis found that (PEI-SA)HA/PC had no significant difference in toxicity between the reproductive organs and the saline group, indicating that (PEI-SA)HA/PC had no significant effect on the reproductive organs. This is consistent with the results of our previously synthesized nanomaterials.[43]

The genital organs were observed by HE staining with light microscopy (Figure 7). There was no significant difference in ovarian and uterus structure between (PEI-SA)HA/PC and the saline group. The ovarian surface

consisted of a single layer of cubic epithelium or flat. The parenchyma of the ovary divides into the peripheral cortex and the central medulla. A variety of follicles, granulosa cells, can be found in the ovarian cortex. The histopathological structure of the uterus showed that the glandular cells were well structured. The stromal cells in both (PEI-SA)HA/PC and saline groups are regular and continuous. It shows that a large number of endometrial gland structures are surrounded by abundant blood vessels.

In the ovarian microstructure (Figure 8), granulosa cells were well observed in both the control group and the (PEI-SA) HA/PC group. The density of the nucleus
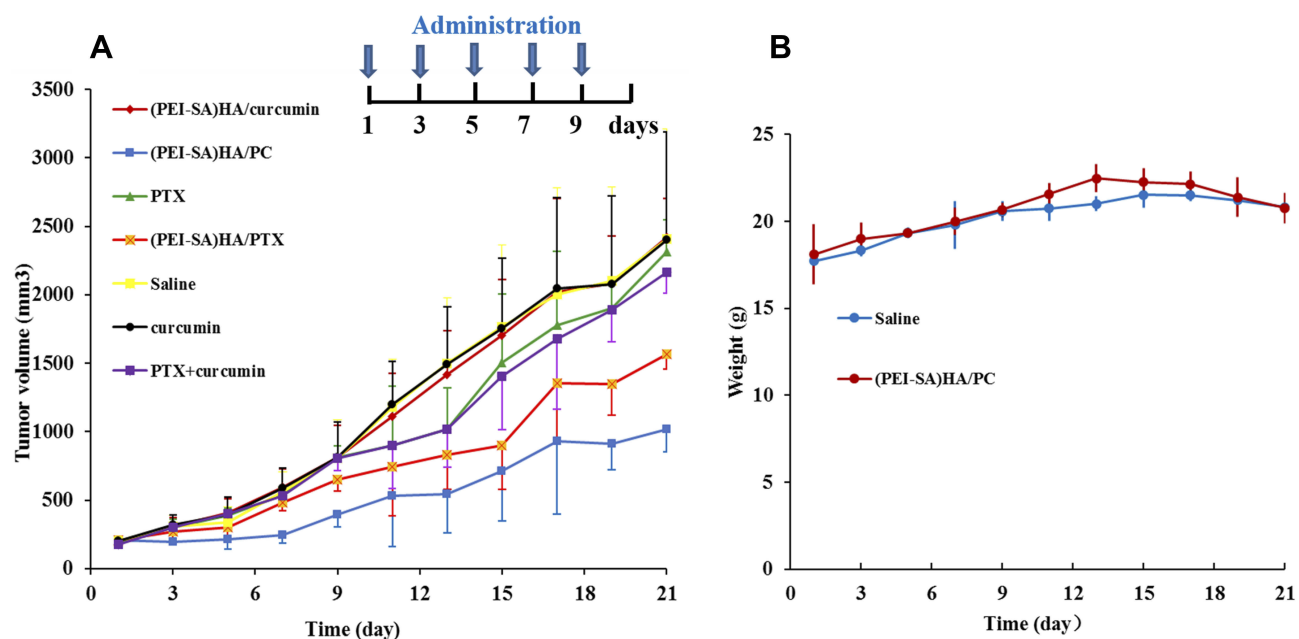
Figure 6 The therapeutic effect of different drugs. (**A**) The volume of tumor in different time in different groups. (**B**) The change in body weight of nude mice in normal saline and (PEI-SA) HA group at different times. There was no significant difference in body weight changes.

Notes: In order to get the statistical significance between every two groups, we use the method of two-sample *t*-test. It showed that the tumor volume of the (PEI-SA)HA/PC group was significantly lower than that of the other groups at 5% level except lower than that of the (PEI-SA)HA/PTX group at 10% level. At the same time, the (PEI-SA)HA/PTX group was only significantly lower than the group of Saline, (PEI-SA)HA/curcumin and curcumin at 10% level.
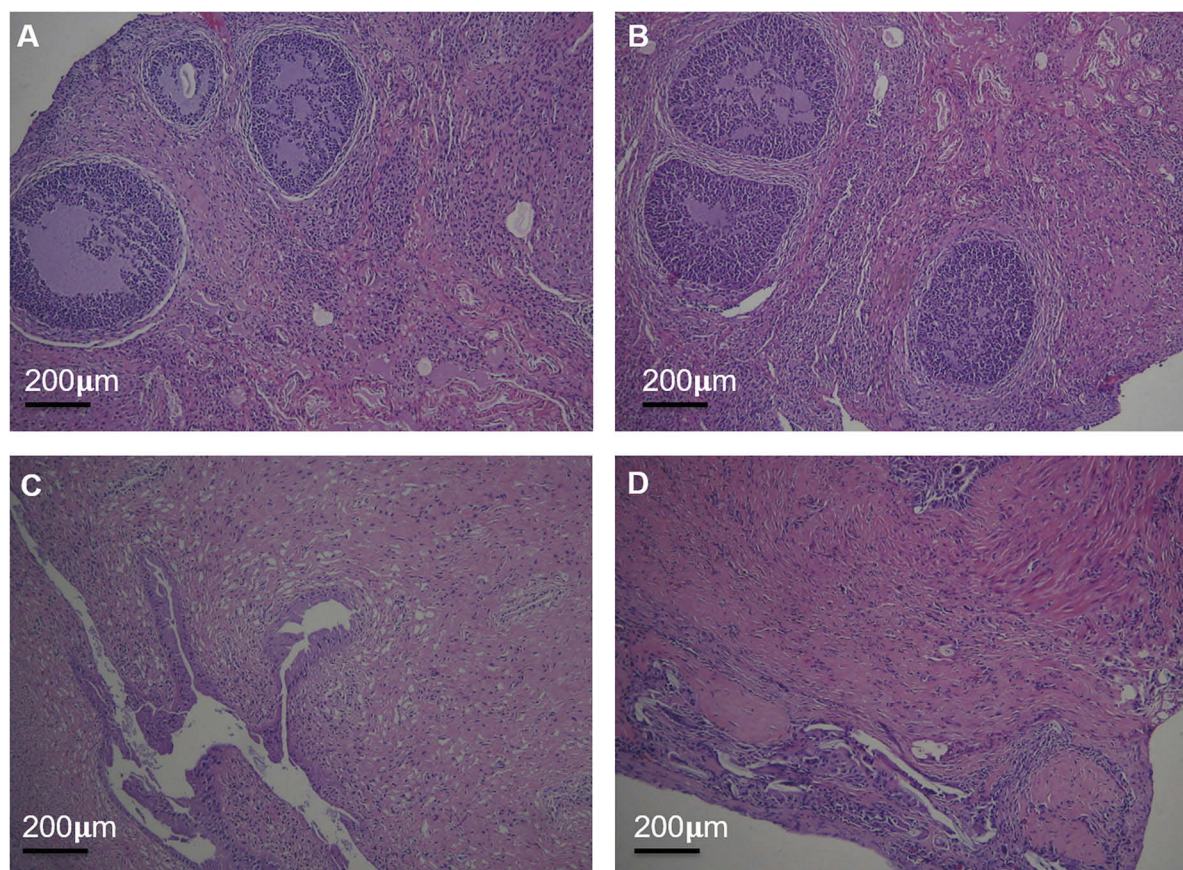

Figure 7 The reproductive organs were examined by HE staining under light microscopy. The structure of the ovary of saline group (**A**) and (PEI-SA)HA/PC group (**B**); the structure of the uterus of saline group (**C**) and (PEI-SA)HA/PC group (**D**). There is no significant difference in ultra-structure between the control group and the (PEI-SA)HA/PC group.
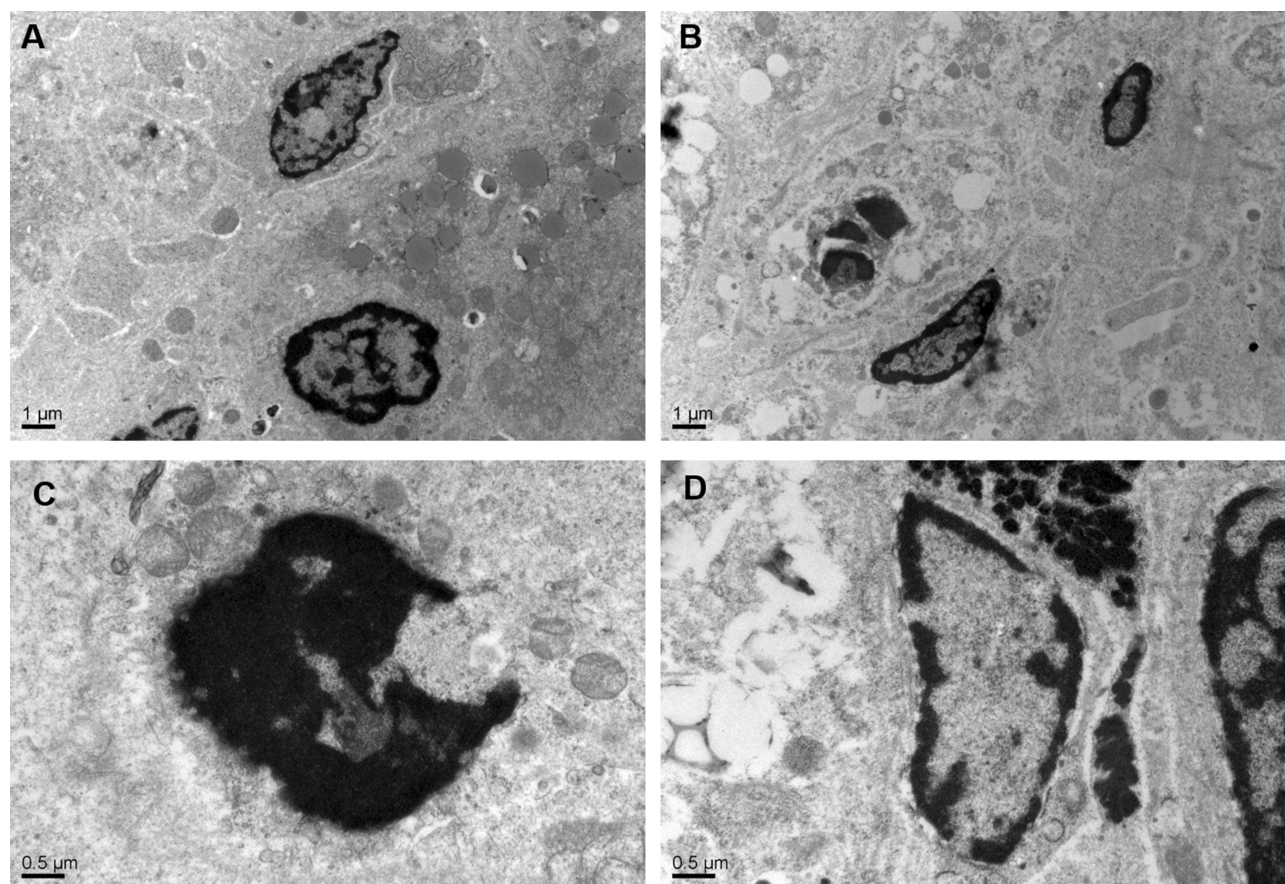
Figure 8 Electron micrograph of uterus and ovarian. Well-preserved morphology and intact nucleus, microvillus structure and abundant villi of the uterus are observed in the saline group (**A**) and (PEI-SA)HA/PC group (**B**). The normal morphology of nucleus can be seen in saline group (**C**) and (PEI-SA)HA/PC group (**D**), apoptotic cells containing nuclear fragments were not found. There is no significant difference in ultra-structure between the control group and the (PEI-SA)HA/PC group.

and matrix is uniform. The cells showed a normal ellipse with a large nucleus, and the endochylema granulocytes are rich in organelles in the literature.[44] This indicates that the cells have normal morphology and microstructure, and there is no typical apoptotic phenomenon. In the microstructure of the uterus, the distribution of blood vessels in the uterus is abundant.[45] In the saline group, many microvilli endometrial glandular epithelial cell surfaces and long villi can be seen. Rich mitochondria, ribosomes, and endoplasmic reticulum can also be observed in the cytoplasm at the same time as the lipid nucleus has prominent nucleoli and intact basement membrane. In the (PEI-SA) HA/PC group, it exhibited the same vascular density, showing abundant villi and microvilli structures. These microscopic view results match the macro perspective. It is stated that no systemic adverse events were observed. The (PEI-SA) HA/PC presented good safety and tolerability. This may still be attributed to the targeting of nanoparticles which reduce the drug adverse reactions.[46–48] This does not mean that (PEI-SA) HA/PC is fully non-toxic, but for adverse drug reactions, some other work can be done to avoid it. Such as, there is a large medical need for biomarkers that predict individual response and susceptibility to toxicity of targeted drugs, which can be used to tailor treatments to reduce the incidence of adverse side effects and improve therapeutic efficacy and safety.[49]

(PEI-SA)HA-mediated curcumin and PTX co-delivery platform could significantly inhibit SKOV3 and SKOV3-TR30 cells from proliferation and invasion in vitro and suppress tumor growth. The findings indicate that (PEI-SA)HA/PC not only increases the role of drugs but also does not increase the adverse drug reactions. In short, (PEI-SA)HA/PC can reverse the drug-resistant treatment of ovarian cancer, which can be used as a promising strategy for therapy ovarian cancer.

Acknowledgments

Disclosure

The authors declare no conflicts of interest in this work.

References

1. Perets R, Drapkin R. It's totally tubular . . ..riding the new wave of ovarian cancer research. *Cancer Res*. 2016;76(1):10–17. doi:10.1158/0008-5472.CAN-15-1382

2. Vallius T, Hynninen J, Kemppainen J, et al. (18)F-FDG-PET/CT based total metabolic tumor volume change during neoadjuvant chemotherapy predicts outcome in advanced epithelial ovarian cancer. *Eur J Nucl Med Mol Imaging*. 2018;45(7):1224–1232. doi:10.1007/s00259-018-3961-z

3. Ju X, Yu H, Liang D, et al. LDR reverses DDP resistance in ovarian cancer cells by affecting ERCC-1, Bcl-2, Survivin and Caspase-3 expressions. *Biomed Pharmacother*. 2018;102:549–554. doi:10.1016/j.biopha.2018.03.092

4. Peng S, Li Z, Zou L, Liu W, Liu C, McClements DJ. Improving curcumin solubility and bioavailability by encapsulation in saponin-coated curcumin nanoparticles prepared using a simple pH-driven loading method. *Food Funct*. 2018;9(3):1829–1839. doi:10.1039/C7FO01814B

5. Li W, Jiang Z, Xiao X, et al. Curcumin inhibits superoxide dismutase-induced epithelial-to-mesenchymal transition via the PI3K/Akt/NF-kappaB pathway in pancreatic cancer cells. *Int J Oncol*. 2018;52(5):1593–1602.

6. Sathe G, Pinto SM, Syed N, et al. Phosphotyrosine profiling of curcumin-induced signaling. *Clin Proteomics*. 2016;13:13. doi:10.1186/s12014-016-9114-0

7. Cheng Y, Zhao P, Wu S, et al. Cisplatin and curcumin co-loaded nano-liposomes for the treatment of hepatocellular carcinoma. *Int J Pharm*. 2018;545(1–2):261–273. doi:10.1016/j.ijpharm.2018.05.007

8. Ma L, Zhang X, Wang Z, et al. Anti-cancer effects of curcumin on myelodysplastic syndrome through the inhibition of enhancer of zeste homolog-2 (EZH2). *Curr Cancer Drug Targets*. 2019. doi:10.2174/1568009619666190212121735

9. Momtazi-Borojeni AA, Mosafer J, Nikfar B, et al. Curcumin in advancing treatment for gynecological cancers with developed drug- and radiotherapy-associated resistance. *Rev Physiol Biochem Pharmacol*. 2018;176:107–129.

10. Tomeh MA, Hadianamrei R, Zhao X. A review of curcumin and its derivatives as anticancer agents. *Int J Mol Sci*. 2019;20(5). doi:10.3390/ijms20051033

11. Kesharwani SS, Ahmad R, Bakkari MA, et al. Site-directed non-covalent polymer-drug complexes for inflammatory bowel disease (IBD): formulation development, characterization and pharmacological evaluation. *J Control Release*. 2018;290:165–179. doi:10.1016/j.jconrel.2018.08.004

12. Kumar S, Kesharwani SS, Mathur H, Tyagi M, Bhat GJ, Tummala H. Molecular complexation of curcumin with pH sensitive cationic copolymer enhances the aqueous solubility, stability and bioavailability of curcumin. *Eur J Pharm Sci*. 2016;82:86–96. doi:10.1016/j.ejps.2015.11.010

13. Kesharwani SS, Kaur S, Tummala H, Sangamwar AT. Overcoming multiple drug resistance in cancer using polymeric micelles. *Expert Opin Drug Deliv*. 2018;15(11):1127–1142. doi:10.1080/17425247.2018.1537261

14. Zhang M, Hagan CTT, Min Y, et al. Nanoparticle co-delivery of wortmannin and cisplatin synergistically enhances chemoradiotherapy and reverses platinum resistance in ovarian cancer models. *Biomaterials*. 2018;169:1–10. doi:10.1016/j.biomaterials.2018.03.055

15. Kesharwani SS, Kaur S, Tummala H, Sangamwar AT. Multifunctional approaches utilizing polymeric micelles to circumvent multidrug resistant tumors. *Colloids Surf B Biointerfaces*. 2019;173:581–590. doi:10.1016/j.colsurfb.2018.10.022

16. Zhao MD, Sun YM, Fu GF, et al. Gene therapy of endometriosis introduced by polymeric micelles with glycolipid-like structure. *Biomaterials*. 2012;33(2):634–643. doi:10.1016/j.biomaterials.2011.09.077

17. Tjhay F, Motohara T, Tayama S, et al. CD44 variant 6 is correlated with peritoneal dissemination and poor prognosis in patients with advanced epithelial ovarian cancer. *Cancer Sci*. 2015;106(10):1421–1428. doi:10.1111/cas.12765

18. Wang J, He H, Xu X, Wang X, Chen Y, Yin L. Far-red light-mediated programmable anti-cancer gene delivery in cooperation with photodynamic therapy. *Biomaterials*. 2018;171:72–82. doi:10.1016/j.biomaterials.2018.04.020

19. Zhao MD, Hu FQ, Du YZ, et al. Coadministration of glycolipid-like micelles loading cytotoxic drug with different action site for efficient cancer chemotherapy. *Nanotechnology*. 2009;20(5):055102. doi:10.1088/0957-4484/20/5/055102

20. Wang XJ, Peng CH, Zhang S, et al. Polysialic-acid-based micelles promote neural regeneration in spinal cord injury therapy. *Nano Lett*. 2019;19(2):829–838. doi:10.1021/acs.nanolett.8b04020

21. Palma DA, Nguyen TK, Louie AV, et al. Measuring the integration of stereotactic ablative radiotherapy plus surgery for early-stage non-small cell lung cancer: a phase 2 clinical trial. *JAMA ONCOL*. 2019;5:681. doi:10.1001/jamaoncol.2018.6993

22. Zehra B, Ahmed A, Sarwar R, et al. Apoptotic and antimetastatic activities of betulin isolated from quercus incana against non-small cell lung cancer cells. *Cancer Manag Res*. 2019;11:1667–1683. doi:10.2147/CMAR.S186956

23. Shi SJ, Wang LJ, Han DH, et al. Therapeutic effects of human monoclonal PSMA antibody-mediated TRIM24 siRNA delivery in PSMA-positive castration-resistant prostate cancer. *Theranostics*. 2019;9(5):1247–1263. doi:10.7150/thno.29884

24. Wu D, Zhang Y, Xu X, et al. RGD/TAT-functionalized chitosan-graft-PEI-PEG gene nanovector for sustained delivery of NT-3 for potential application in neural regeneration. *Acta Biomater*. 2018;72:266–277. doi:10.1016/j.actbio.2018.03.030

25. Andrade S, Ramalho MJ, Pereira MDC, Loureiro JA. Resveratrol brain delivery for neurological disorders prevention and treatment. *Front Pharmacol*. 2018;9:1261. doi:10.3389/fphar.2018.01261

26. Que X, Su J, Guo P, et al. Study on preparation, characterization and multidrug resistance reversal of red blood cell membrane-camouflaged tetrandrine-loaded PLGA nanoparticles. *Drug Deliv*. 2019;26(1):199–207. doi:10.1080/10717544.2019.1573861

27. Alsaab HO, Sau S, Alzhrani RM, et al. Tumor hypoxia directed multimodal nanotherapy for overcoming drug resistance in renal cell carcinoma and reprogramming macrophages. *Biomaterials*. 2018;183:280–294. doi:10.1016/j.biomaterials.2018.08.053

28. Li N, Liu YY, Li Y, et al. Fine tuning of emission behavior, self-assembly, anion sensing, and mitochondria targeting of pyridinium-functionalized tetraphenylethene by alkyl chain engineering. *ACS Appl Mater Interfaces*. 2018;10(28):24249–24257. doi:10.1021/acsami.8b04113

29. Wang W, Zhang K, Chen D. From tunable DNA/polymer self-assembly to tailorable and morphologically pure core-shell nanofibers. *Langmuir*. 2018;34(50):15350–15359. doi:10.1021/acs.langmuir.8b02992

30. Dong Q, Zhang H, Han Y, et al. Tumor environment differentiated "nanodepot" programmed for site-specific drug shuttling and combinative therapy on metastatic cancer. *J Control Release*. 2018;283:59–75. doi:10.1016/j.jconrel.2018.05.027

31. Kalyane D, Raval N, Maheshwari R, Tambe V, Kalia K, Tekade RK. Employment of enhanced permeability and retention effect (EPR): nanoparticle-based precision tools for targeting of therapeutic and diagnostic agent in cancer. *Mater Sci Eng C Mater Biol Appl*. 2019;98:1252–1276. doi:10.1016/j.msec.2019.01.066

32. Liang C, Chao Y, Yi X, et al. Nanoparticle-mediated internal radioisotope therapy to locally increase the tumor vasculature permeability for synergistically improved cancer therapies. *Biomaterials*. 2019;197:368–379. doi:10.1016/j.biomaterials.2019.01.033

33. Wang Q, Zhong Y, Liu W, et al. Enhanced chemotherapeutic efficacy of the low-dose doxorubicin in breast cancer via nanoparticle delivery system crosslinked hyaluronic acid. *Drug Deliv*. 2019;26 (1):12–22. doi:10.1080/10717544.2018.1507057

34. Carvalho AM, Teixeira R, Novoa-Carballal R, Pires RA, Reis RL, Pashkuleva I. Redox-responsive micellar nanoparticles from glycosaminoglycans for CD44 targeted drug delivery. *Biomacromolecules*. 2018;19(7):2991–2999. doi:10.1021/acs.biomac.8b00561

35. Hossaini Nasr S, Tonson A, El-Dakdouki MH, et al. Effects of nanoprobe morphology on cellular binding and inflammatory responses: hyaluronan-conjugated magnetic nanoworms for magnetic resonance imaging of atherosclerotic plaques. *ACS Appl Mater Interfaces*. 2018;10(14):11495–11507. doi:10.1021/acsami.7b19708

36. Hu L, Li M, Zhang Z, Shen Y, Guo S. Self-assembly of biotinylated poly (ethylene glycol)-poly(curcumin) for paclitaxel delivery. *Int J Pharm*. 2018;553(1–2):510–521. doi:10.1016/j.ijpharm.2018.10.019

37. Fratantonio D, Molonia MS, Bashllari R, et al. Curcumin potentiates the antitumor activity of Paclitaxel in rat glioma C6 cells, Phytomedicine: international. *Phytomedicine*. 2018;55:23–30. doi:10. 1016/j.phymed.2018.08.009

38. Alemi A, Zavar Reza J, Haghiralsadat F, et al. Paclitaxel and curcumin coadministration in novel cationic PEGylated niosomal formulations exhibit enhanced synergistic antitumor efficacy. *J Nanobiotechnology*. 2018;16(1):28. doi:10.1186/s12951-018-0351-4

39. Yang Z, Sun N, Cheng R, et al. pH multistage responsive micellar system with charge-switch and PEG layer detachment for co-delivery of paclitaxel and curcumin to synergistically eliminate breast cancer stem cells. *Biomaterials*. 2017;147:53–67. doi:10.1016/j.biomaterials.2017.09.013

40. Yao Q, Gutierrez DC, Hoang NH, et al. Efficient codelivery of paclitaxel and curcumin by novel bottlebrush copolymer-based micelles. *Mol Pharm*. 2017;14(7):2378–2389. doi:10.1021/acs.molpharmaceut.7b00278

41. Calaf GM, Ponce-Cusi R, Carrion F. Curcumin and paclitaxel induce cell death in breast cancer cell lines. *Oncol Rep*. 2018;40 (4):2381–2388. doi:10.3892/or.2018.6603

42. Gawde KA, Sau S, Tatiparti K, et al. Paclitaxel and di-fluorinated curcumin loaded in albumin nanoparticles for targeted synergistic combination therapy of ovarian and cervical cancers. *Colloids Surf B Biointerfaces*. 2018;167:8–19. doi:10.1016/j.colsurfb.2018.03.046

43. Zhao MD, Cheng JL, Yan JJ, et al. Hyaluronic acid reagent functional chitosan-PEI conjugate with AQP2-siRNA suppressed endometriotic lesion formation. *Int J Nanomedicine*. 2016;11:1323–1336. doi:10.21 47/IJN.S99692

44. Biswas P, Mukhopadhyay A, Kabir SN, Mukhopadhyay PK. High-protein diet ameliorates arsenic-induced oxidative stress and antagonizes uterine apoptosis in rats. *Biol Trace Elem Res*. 2019;192: 222–233. doi:10.1007/s12011-019-1657-2

45. Camozzato GC, Martinez MN, Bastos HBA, et al. Ultrastructural and histological characteristics of the endometrium during early embryo development in mares. *Theriogenology*. 2019;123:1–10. doi:10.1016/ j.theriogenology.2018.09.018

46. Zhou J, Li M, Lim WQ, et al. A transferrin-conjugated hollow nanoplatform for redox-controlled and targeted chemotherapy of tumor with reduced inflammatory reactions. *Theranostics*. 2018;8 (2):518–532. doi:10.7150/thno.21194

47. Zou H, Zhu J, Huang DS. Cell membrane capsule: a novel natural tool for antitumour drug delivery. *Expert Opin Drug Deliv*. 2019;16 (3):1–19.

48. Tang X, Wang G, Shi R, et al. Enhanced tolerance and antitumor efficacy by docetaxel-loaded albumin nanoparticles. *Drug Deliv*. 2016;23(8):2686–2696. doi:10.3109/10717544.2015.1049720

49. Hattinger CM, Patrizio MP, Luppi S, Magagnoli F, Picci P, Serra M. Current understanding of pharmacogenetic implications of DNA damaging drugs used in osteosarcoma treatment. *Expert Opin Drug Metab Toxicol*. 2019;15:299–311. doi:10.1080/17425255.2019.1588885